Biosensors and Bioelectronics 171 (2021) 112707

Contents lists available at ScienceDirect

Biosensors and Bioelectronics

journal homepage: http://www.elsevier.com/locate/bios

Label-free homogeneous electrochemical detection of MicroRNA based on target-induced anti-shielding against the catalytic activity of two-dimension nanozyme

Jiahui Wu, Wenxin Lv, Qiaoting Yang, Haiyin Li **, Feng Li *

College of Chemistry and Pharmaceutical Sciences, Qingdao Agricultural University, Qingdao, 266109, People's Republic of China

ARTICLE INFO

Keywords:
2D MnO_2 nanoflakes
Nanozymes
Homogeneous electrochemical
Oxidase- and peroxidase-like properties

ABSTRACT

In traditional homogeneous electrochemical sensing system, methylene blue was stricken with nonspecific intercalation and weak stability, inevitably distorting the diagnosis results. Given the unique catalytic activity of oxidase- and peroxidase-like nanozymes, it is interesting to develop a nanozyme-based homogeneous electrochemical biosensor. Whereas, the preparation of nanozymes with dual enzyme-like activities and two dimensional (2D) morphology is a great challenge. Herein, a soft template-directed wet chemical approach was proposed for preparation of 2D MnO_2 nanoflakes, in which the morphology can be easily tuned by the template dosage. Interestingly, not only the oxidase-like activity was discovered, but 2D MnO_2 nanoflakes also display a significant peroxidase-like activity. Noticeably, 2D MnO_2 nanoflakes exhibit superior response to single stranded deoxyribonucleic acid (ssDNA) over double stranded DNA in the aspect of binding and catalytic activity, which triggers a highly sensitive homogeneous electrochemical detection of microRNA. This study about finding nanozymes with dual enzyme-like activities and ssDNA with inhibiting effect will set up a new avenue to extend the application range of nanozymes and throws a new light on the development of higher-performance electrochemical biosensors.

1. Introduction

As a simple, rapid and sensitive analytical methodology, electrochemical biosensor has fascinated substantial concerns in the areas of disease diagnosis (Lin et al., 2018; Bai et al., 2020), food safety analysis (Jong et al., 2016; Martinfernandez et al., 2017; Silva et al., 2018) and environmental safety management (Taylor et al., 2012; Yan et al., 2013). Very recently, homogeneous electrochemical biosensors have attracted more and more interest because of their independence of high-cost and complex immobilization, which makes the detection reaction happen in homogeneous solution rather than the electrodes' surface, effectively avoiding the influence of steric hindrance effect of electrode on reactive activity of biological receptors, and thus maximally improving the recognition efficiency, as well as the sensing performance. In homogeneous electrochemical system, methylene blue (MB) is usually applied as a signal indicator through varying the configuration of deoxyribo nucleic acid (DNA), subsequently changing the exiting form of MB (Chang et al., 2020; Hou et al., 2015). Unfortunately, current approaches may distort the results, because MB can intercalate into aleatoric double stranded DNA (Li et al., 2020), G-quadruplex DNA (Zhang et al., 2014) and others, and the produced MB-based composites are weakly stable. Therefore, seeking a higher-efficiency strategy for changing the existing forms of MB has been placed on the agenda.

In comparison with previous strategies, reaction-based approach may be a potential candidate for ideal homogeneous electrochemical biosensors development (Zhao et al., 2013; Wang et al., 2018; Xing et al., 2011; Wiedmer et al., 2016). However, it needs to be seriously considered how to efficiently eliminate MB. Previously reported works demonstrate H_2O_2-involved catalytic oxidation might be the most popular method (Xing et al., 2011; Wiedmer et al., 2016). It generated reactive oxygen species (ROS) in the presence of metal or metal oxide or other nanostructures, and the formed ROS could efficiently eliminate MB through catalytic oxidation reaction. Besides, for a strategy to be suitable trigger for detection application, it must proceed with excellent biocompatibility. Nevertheless, H_2O_2 is poisonous and easily volatile.

* Corresponding author.
** Corresponding author.
E-mail addresses: lihaiyin@qau.edu.cn (H. Li), lifeng@qau.edu.cn (F. Li).

https://doi.org/10.1016/j.bios.2020.112707
Received 1 August 2020; Received in revised form 16 September 2020; Accepted 6 October 2020
Available online 8 October 2020

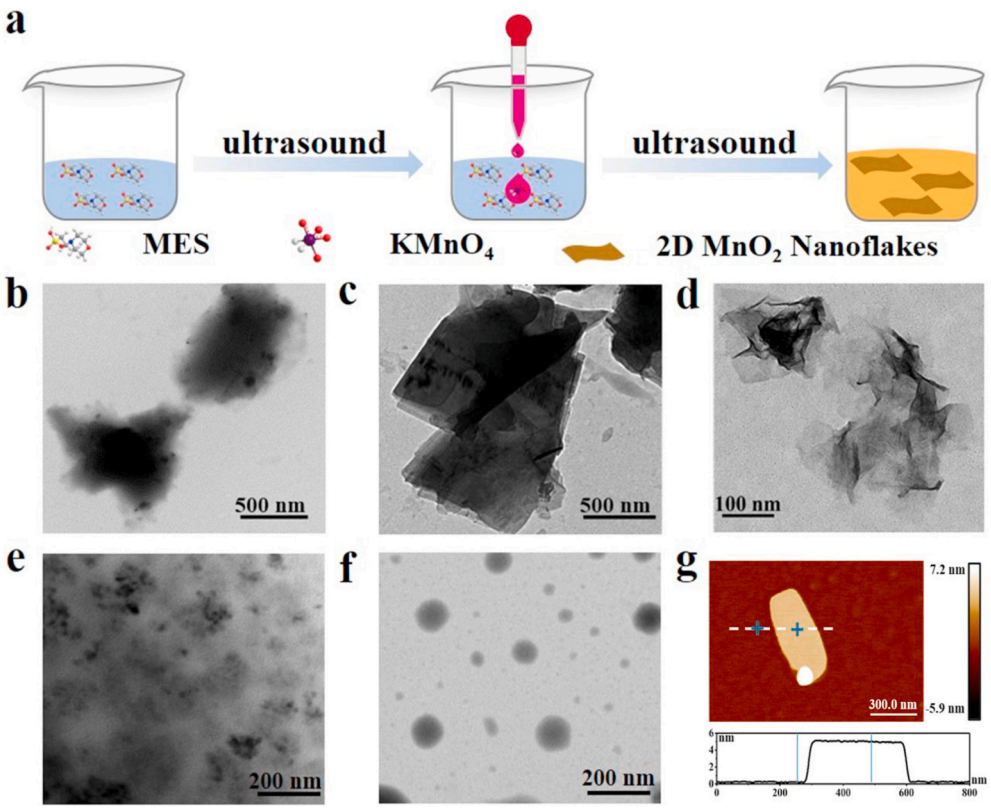

Fig. 1. (a) Scheme illustration of the fabrication of 2D MnO_2 nanoflakes. (b)–(f) TEM images of the MnO_2 nanomaterials by using different dosages of MES: 0.001, 0.01, 0.1, 1.0 and 2.0 M. (g) AFM image of 2D MnO_2 nanoflakes.

Looking for an enduring and biocompatible reagent as an alternative to H_2O_2 is highly desirable. O_2, existing in the solution, has the superior stability and biocompatibility to H_2O_2, and thus can be acted as an ideal candidate. Unfortunately, the elimination efficiency of MB by O_2 is ultralow, and thus O_2 is not conductive to MB-based homogeneous electrochemical biosensors. Hence, how to promote the activation of O_2 to produce ROS is largely important.

In the wake of developments in enzyme engineering and nanotechnology, nanomaterials with the capability of mimicking the natural enzymes' function emerge (called as nanozymes), and can act as substitutes of natural enzymes because of the stronger stability, higher catalytic activity, as well as lower price and simpler preparation (Wu et al., 2019; Huang et al., 2019; Qiu et al., 2018; Zhang et al., 2019; Han et al., 2018; Li et al., 2019; Xi et al., 2019; Wang et al., 2017; Fu et al., 2019; Chen et al., 2019; Weerathunge et al., 2019; Singh et al., 2017; Kang et al., 2019; Palomo, 2019; Kim et al., 2020). However, most works exist on the use of nanozymes in colorimetric biosensing (Han et al., 2018; Li et al., 2019; Liu et al., 2012), antibiosis (Xi et al., 2019; Liu et al., 2019), and disease treatment (Wang et al., 2017; Fu et al., 2019; Chen et al., 2019). The research of nanozymes in homogeneous electrochemical system remains blank. Recently, it was found that nanozymes could activate O_2 into ROS. While most nanozymes possess the single enzyme-like activity (Li et al., 2019; Weerathunge et al., 2019) rather than dual/multiple enzyme-like activities (Han et al., 2018; Liu et al., 2019). Dual/multiple enzyme-like activities endow nanozymes with higher activation efficiency of O_2. Besides, an effective reaction-based homogeneous electrochemical biosensor must respond specifically to its intended analyte, and thus the elimination process of MB must proceed selectively. Profiting from the deep investigation of interaction of two dimensional (2D) nanomaterials and bioreceptors, it revealed that 2D nanomaterials could selectively adsorb ssDNA against dsDNA (Weerathunge et al., 2019; Liu et al., 2012). Furthermore, 2D nanomaterials possess ultrathin thickness and high surface area. If there is a nanozyme with 2D morphology (2D nanozyme), selective elimination of MB will be assured through adjusting the amount of ssDNA adsorbed. Moreover, most nanozymes have the morphologies of nanocluster (Singh et al., 2017; Kang et al., 2019) and nano/micro-particle (Palomo, 2019) rather than 2D morphology. Therefore, discovery of a 2D nanozyme with dual/multiple enzyme-like activities becomes essential, but remains a great challenge.

Herein, we develop a soft template-directed wet chemical approach for controllable preparation of 2D MnO_2 nanoflakes with dual enzyme-like activities, and we further apply them in construction of a homogeneous electrochemical biosensing system. Soft template-directed wet chemical synthesis is beneficial for one-step and large-scale production of uniform-sized nanomaterials and has the advantages of low cost, environmental friendliness, and wide applicability (Zhou et al., 2014). The morphologies and enzyme-like activities of MnO_2 can be tuned by varying the molar ratio between $KMnO_4$ and 2-(N-morpholino) ethanesulfonic acid (MES). The 2D MnO_2 nanoflakes behave superior efficiency to activate the dissolved O_2 into ROS because of the oxidase- and peroxidase-like activities. Furthermore, by van der Waals interaction, $P_{let\text{-}7a}$ was adsorbed on the surface of 2D MnO_2 nanoflakes, and more interestingly, $P_{let\text{-}7a}$ obviously declined the enzyme-like activities through masking the surface active sites and prohibiting them from coming into contact with substrates. Synergy with the superior binding to ssDNA over dsDNA, 2D MnO_2 nanoflakes was exploited to homogeneously electrochemical detect microRNA (miRNA), using let-7a as the proof-of-concept analyte.

2. Results and discussion

2.1. Characterization of 2D MnO_2 nanoflakes

Fig. 1a gives the illustration of fabrication of 2D MnO_2 nanoflakes through a soft template-directed wet chemical approach. Concisely, 25

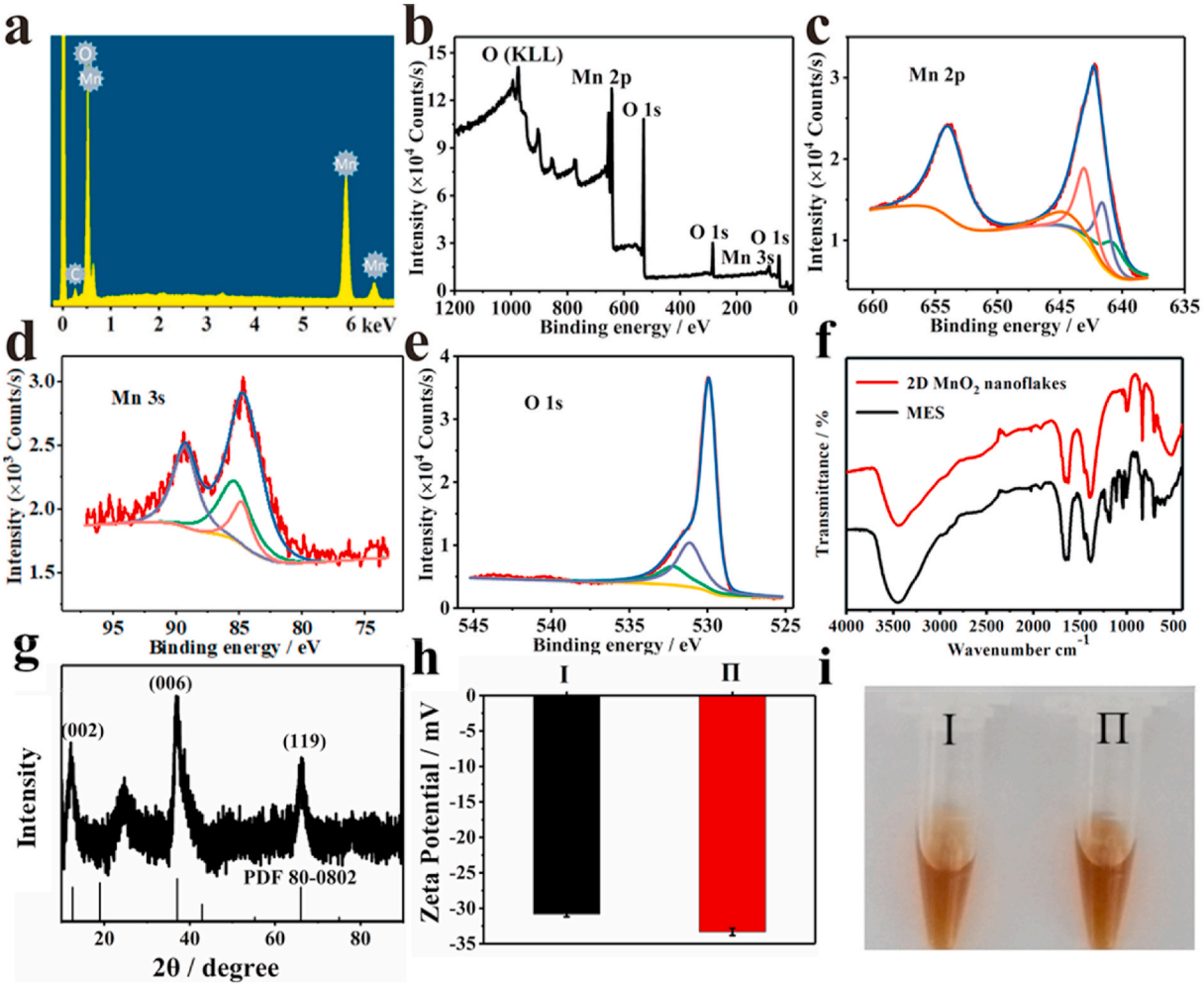

Fig. 2. EDS (a) and XPS (b) spectra of 2D MnO_2 nanoflakes. High-resolution XPS pattern of Mn 2p (c), Mn 3s (d) and O 1s (e). (f) FT-IR spectra of MES and 2D MnO_2 nanoflakes. (g) PXRD curve of 2D MnO_2 nanoflakes and PDF 80–0802. (h) Zeta potential value of 2D MnO_2 nanoflakes (I) and $P_{let\text{-}7a}/MnO_2$ (II). (i) Images of 26 μg/mL 2D MnO_2 nanoflakes (I) and $P_{let\text{-}7a}/MnO_2$ (800 nM $P_{let\text{-}7a}$ and 26 μg/mL 2D MnO_2 nanoflakes, II) dispersed in PBS.

mL of water solution containing 0.01 M $KMnO_4$ was added into 25 mL of water solution containing 0.1 M MES under ultrasonic condition. MES served as both of the soft template and reducing agent. To acquire a well-defined 2D morphology, the amount of MES was cautiously discussed ranging from 0.001, 0.01, 0.1, 1.0 to 2.0 M, and the morphologies of MnO_2 samples were evaluated by transmission electron microscope (TEM) and atomic force microscope (AFM). Irregular shape was observed at a low MES dosage (0.001 and 0.01 M in Fig. 1b and c), and a well-defined 2D morphology was determined when increasing MES concentration to 0.1 M (Fig. 1d). The lateral dimension and thickness of 2D MnO_2 nanoflakes were calculated to be 300 nm and 5 nm, respectively (Fig. 1g). Nevertheless, with MES dosage further increasing, the morphology transformed nanoflakes to sphere-like nanostructures (Fig. 1e and f), probably due to the reason that too many MES supplied profuse nucleation sites and prevented the interconnection of MnO_2 phase. These information clarified that 2D MnO_2 nanoflakes could be precisely fabricated by adjusting the dosage of MES.

To research the compositions and valence states of the products, energy-dispersive X-ray spectroscopy (EDS), X-ray photoelectron spectroscopy (XPS), and power X-ray diffraction (PXRD) were carried out. Sharp peaks in EDS and XPS curves implied that Mn and O elements are the main components (Fig. 2a and b). Besides, a EDS peak located at 0.27 keV, corresponding to C element, was also observed, judging the presence of MES. Further, Mn 2p peaks were deconvoluted into two constituents, 2p 1/2 peak (654.02 eV) and 2p 3/2 peak (642.23 eV), and the spin energy separation was calculated to be 11.79 eV (Fig. 2c). For Mn 3s peak, the energy separation was determined to be 4.69 eV (Fig. 2d); for O 1s, the XPS peak was recorded at 530 eV, proving Mn–O bonds (Fig. 2e). Both measured peaks and energy separations justified the existence of MnO_2 in the fabricated nanostructures. Meanwhile, three sharp peaks at 12.30°, 37.10° and 66.15° appeared in PXRD curve (Fig. 2g), which were ascribed to (002), (006), and (109) crystal planes of birnessite-type MnO_2 (PDF 80–0802), respectively. Fourier transform infrared spectra (FT-IR) spectra demonstrated that 2D MnO_2 nanoflakes displayed the peak at 1382 cm^{-1} and 992 cm^{-1}, which were typical values for sulfonic group and could also be found in the curve of MES, suggesting the existence of MES on the surface (Fig. 2f). The existed MES made the negative zeta potential increase to −30.30 mV (Fig. 2h), which indicated the excellent dispersibility. As expected, 2D MnO_2 nanoflakes were uniformly dispersed in phosphate-buffered saline (PBS) without any precipitates for 2.0 h (Fig. 2i–I). Meanwhile, the obvious negative potential facilitated their high affinity to positive substrates, such as 3,3′,5,5′-tetramethylbenzidine (TMB), methylene blue (MB), and o-phenylenediamine (OPD), further enhancing the enzyme-like activities.

2.2. Discovery of enzyme-like activities

To discover the dual enzyme-like activities of as-fabricated 2D MnO_2 nanoflakes, enzymatic substrates including TMB, OPD, and 2,2-azinobis (3-ethylbenzthiazoline-6-sulfonic acid (ABTS) were individually added

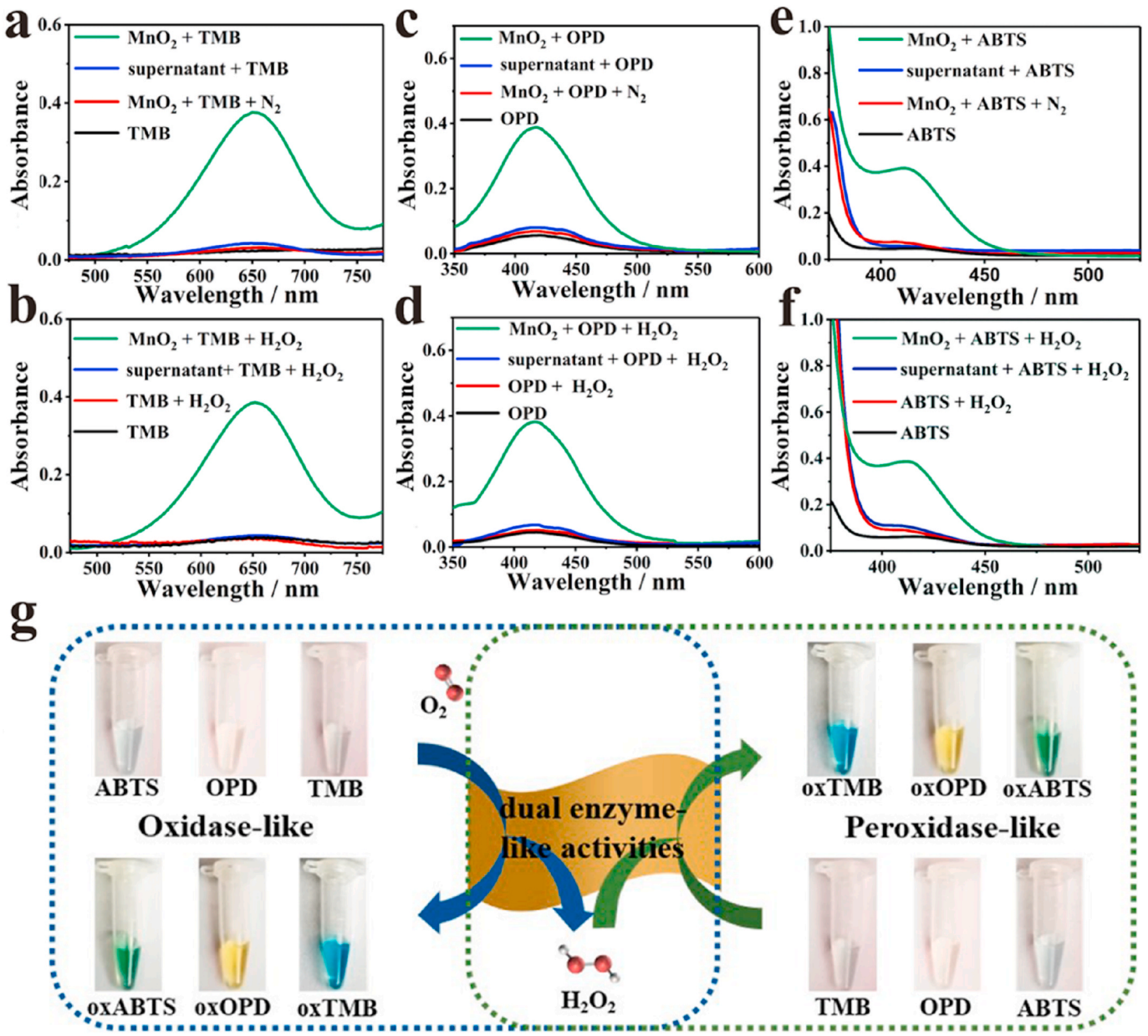

Fig. 3. Typical UV-vis spectra of TMB (a), OPD (c), and ABTS (e) catalyzed oxidation based on oxidase-like activity of 2D MnO_2 nanoflakes and contrasts. Typical UV-vis spectra of TMB (b), OPD (d), and ABTS (f) catalyzed oxidation based on peroxidase-like activity of 2D MnO_2 nanoflakes and contrasts in deoxidized PBS. (g) Schematic illustration of interaction of 2D MnO_2 nanoflakes and enzymatic substrates based on oxidase-like and peroxidase-like activities. The concentrations of TMB, OPD, and ABTS are 0.5 mM, and the concentration of 2D MnO_2 nanoflakes is 2.6 μg/mL.

into the reaction solution under different conditions. The oxidase-like activity was first evaluated. As illustrated in Figs. 2 and 3a D MnO_2 nanoflakes-catalyzed reaction solution displayed a highly significant peak of oxidized TMB (oxTMB) at 652 nm, however slight absorbance could be determined without 2D MnO_2 nanoflakes. For an oxidase-involved catalytic oxidation reaction, O_2 acts as an indispensable component. To validate this, the reaction solution was deoxidized by N_2. Owing to the absence of O_2, the reaction solution exhibited inappreciable absorbance at 652 nm in the presence of 2D MnO_2 nanoflakes. To verify the matter capable of catalyzing oxidation of TMB into oxTMB is the 2D MnO_2 nanoflakes rather than released free manganese ions, 2D MnO_2 nanoflakes were soaked in PBS for 4.0 h, and subsequently, the supernatant was gotten through centrifugation and replaced 2D MnO_2 nanoflakes to react with TMB. Ultraviolet and visible (UV-vis) spectrum demonstrated that the supernatant-catalyzed reaction solution displayed ultralow absorbance at 652 nm, which was approximately identical with that of TMB alone. Similar variation phenomena for OPD and ABTS at 417 nm and 413 nm were also recorded (Fig. 3c and e). Taken together, the prepared 2D MnO_2 nanoflakes possessed distinguished oxidase-like activity and substrate versatility, keeping good line with those of reported nanozymes with oxidase-like activity and natural oxidase.

Further, the peroxidase-like property of 2D MnO_2 nanoflakes was investigated using H_2O_2 as the substitute for O_2 in the reaction of TMB, OPD, and ABTS oxidation. The UV-vis spectra in Fig. 3b demonstrated that TMB was obviously oxidized under the catalysis of 2D MnO_2 nanoflakes rather than released free manganese ions. For OPD and ABTS, similar changes in absorbance were also gotten (Fig. 3d and f). These data evidenced the outstanding peroxidase-like activity of 2D MnO_2 nanoflakes. On the basis of the dual enzyme-like activities, i.e., oxidase activity and peroxidase activity, the interaction mechanism between 2D MnO_2 nanoflakes and enzymatic substrates was deduced as

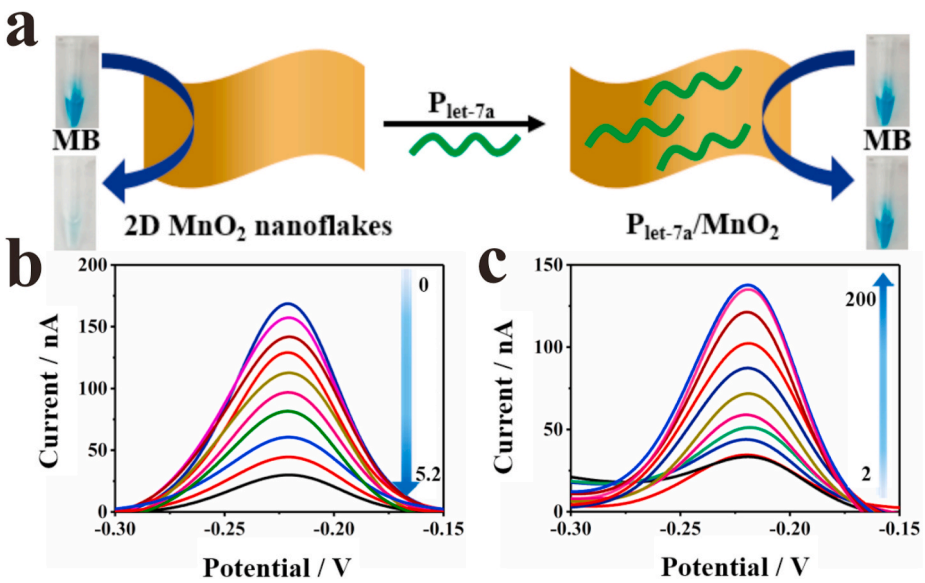

Fig. 4. (a) Effect of $P_{let\text{-}7a}$ on the catalytic activity of 2D MnO_2 nanoflakes toward MB. (b) DPV curves of MB (1.4 μM) catalyzed oxidation by 2D MnO_2 nanoflakes with different concentrations: 0, 0.5, 1.0, 1.6, 2.2, 2.8, 3.4, 4.0, 4.6, and 5.2 μg/mL. (c) DPV curves of MB (1.4 μM) catalyzed oxidation by 2D MnO_2 nanoflakes (5.2 μg/mL) with different concentrations of $P_{let\text{-}7a}$: 2, 5, 10, 16, 24, 40, 60, 80, 120, 160, and 200 nM.

manifested in Fig. 3g. 2D MnO_2 nanoflakes catalyzed oxidation of TMB/OPD/ABTS into oxTMB/oxOPD/oxABTS in the presence of O_2 by making full use of the oxidase-like activity, as well as O_2 was reduced into H_2O_2; the yielded H_2O_2 was applicable for subsequent peroxidase-initiated catalytic oxidation; thus, the reaction solution transformed colorless into blue, yellow, and green for TMB, OPD, and ABTS, respectively. In this context, the dual enzyme-like activities of 2D MnO_2 nanoflakes facilitate their high efficiency to catalyze oxidation of enzymatic substrates, benefiting the highly efficient elimination of MB.

For advanced application of 2D MnO_2 nanoflakes in analytical field, the effect of temperature and pH value on catalytic activity was researched. As depicted in Fig. S1, MnO_2 nanoflakes displayed >90% of the relative activity when the temperature was ≤50 °C, whereas significantly declined activity was observed with the temperature further elevating. Changing pH value from 1.0 to 10.0, it was found from Fig. S2 that 2D MnO_2 nanoflakse exhibited >80% of the relative activity in the pH range of 3.0–7.0. When the pH value was smaller than 3.0 or larger than 7.0, the catalytic activity abruptly decreased. The reduce caused by high temperature and excessively low/high pH value might be due to the decomposition of 2D MnO_2 nanoflakes, which can be confirmed by TEM characterizations (Fig. S3). Overall, the prepared 2D MnO_2 nanoflakes possessed more splendid thermal and pH stability than bioenzymes.

To protrude the advantage of 2D MnO_2 nanoflakes in oxidation catalysis, other MnO_2 materials prepared from different MES dosage were employed as contrast substances to react with TMB under the same conditions with 2D MnO_2 nanoflakes (Fig. S4). After the reaction, the absorbance at 652 nm raised to 0.178, 0.233, 0.268 and 0.207 for 0.001, 0.01, 1.0, and 2.0 M of MES, respectively, which are smaller than that of 0.1 M of MES, suggesting the lower catalytic efficiency of other MnO_2 materials than 2D MnO_2 nanoflakes. The reason might be ascribed to the ultrathin thickness, large surface area and high negative surface charge, permitting rapid electron transfer, sufficient contact and interaction with TMB. Moreover, with the dosage of 2D MnO_2 nanoflakes elevating, the absorbance gradually accelerated, suggesting the catalytic oxidation was mainly relied on the amount of 2D MnO_2 nanoflakes; with the reaction time increasing, the absorbance gradually raised and levelled off at 100 s, implying a rapid response (Fig. S5).

2.3. Development of 2D MnO_2 nanoflakes-based homogeneous electrochemical biosensor

As is well known, nanozymes are mainly applied as colorimetric sensors for sensitive detection of H_2O_2 (Kim et al., 2020), glucose (Han et al., 2018), and metal ions (Liu et al., 2017). In comparison with colorimetric sensors, homogeneous electrochemical sensors have attracted more attention due to their higher sensitivity and faster response. It is of significant interest to explore nanozymes-based homogeneous electrochemical sensors, but remains a challenge. The main reasons was ascribed to the following aspects: how to selectively eliminate MB, how to have the recognizable units, and how to broaden the application scope. With this in mind, we first investigate whether 2D MnO_2 nanoflakes can eliminate MB. The experiment was performed by incubating MB with 2D MnO_2 nanoflakes at different dosages (Fig. 4a). After the reaction, the blue color became shallow. The DPV curves in Fig. 4b demonstrated that the peak current gradually declined with the dosage of 2D MnO_2 nanoflakes elevating. Similar variation trend of absorbance was also be found in Fig. S6. These results indicated the elimination of MB and justified the catalytic oxidation ability of 2D MnO_2 nanoflakes on MB.

The response of 2D MnO_2 nanoflakes to ssDNA was researched through the incubation of $P_{let\text{-}7a}$ with 2D MnO_2 nanoflakes ($P_{let\text{-}7a}$/MnO_2), and $P_{let\text{-}7a}$ was closely adsorbed on the surface of 2D MnO_2 nanoflakes due to the hydrogen bond and π-π stacking, thus causing negligible color variation for MB (Fig. 4a). As illustrated in Fig. 4c and S7a, the absorbance at 655 nm and DPV current at −0.219 V were low in the reaction solution comprising 2D MnO_2 nanoflakes and MB. In sharp contrast, after the addition of $P_{let\text{-}7a}$, the absorption and DPV peak intensities significantly heightened, and with the dosage of $P_{let\text{-}7a}$ elevating, the output signals gradually raised. Similar results could also be gotten for TMB, OPD and ABTS in Fig. S7b-d, respectively. These variations in absorbance and DPV current obviously evidenced that ssDNA could decline the catalytic activity of 2D MnO_2 nanoflakes through masking the surface active sites and prohibiting them from coming into contact with substrates. Besides, $P_{let\text{-}7a}$/MnO_2 also has the unprecedented dispersibility obtained from the high negative potential (−33.33 mV) and image in Fig. 2i–II. Furthermore, the optimum incubation time and dosage of $P_{let\text{-}7a}$ were calculated to be 30 min and 160 nM, respectively (Fig. S8).

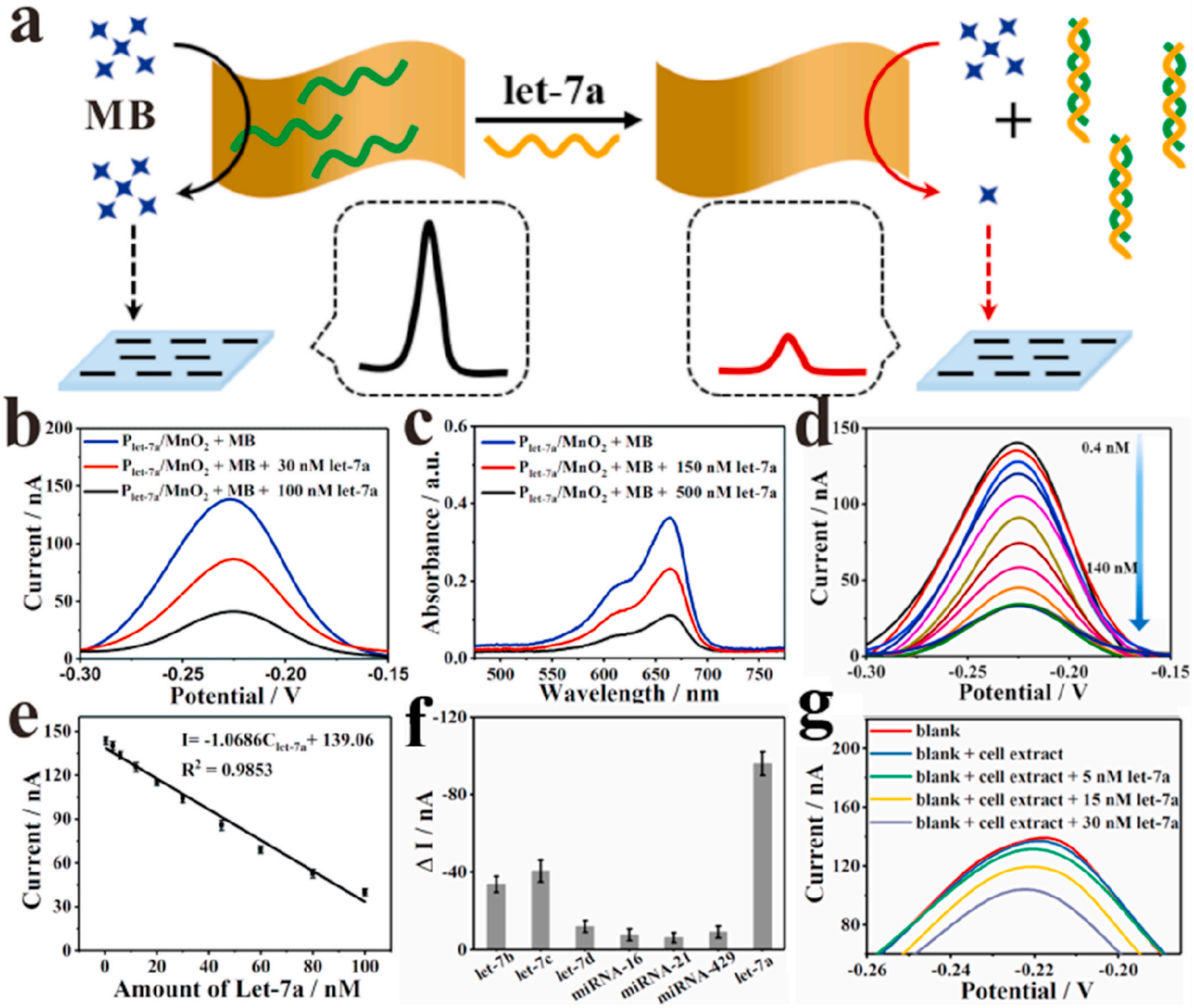

Fig. 5. (a) Sensing principle of P_{let-7a}/MnO_2-based homogeneous electrochemical biosensor for miRNA assay. DPV (b) and UV-vis (c) curves of MB catalyzed oxidation by P_{let-7a}/MnO_2 in the presence of let-7a with different concentrations. (d) Typical DPV curves of MB catalyzed oxidation by P_{let-7a}/MnO_2 corresponding to let-7a with different dosages: 0.4, 2, 6, 12, 20, 30, 44, 60, 80, 100, 120 and 140 nM. (e) Linear relationship between DPV peak current and let-7a dosage. (f) Selectivity experiment of P_{let-7a}/MnO_2-based homogeneous electrochemical biosensor. The concentrations of all miRNAs were 100 nM. (g) DPV curves of MB catalyzed oxidation by P_{let-7a}/MnO_2 upon the addition of cell extract.

On the basis of the above-described information, P_{let-7a}/MnO_2 was employed to sensitively detect microRNA (miRNA), using let-7a as the target object. To our best knowledge, there has been no documented example of nanozymes-based homogeneous electrochemical analysis for miRNA. The working mechanism for miRNA assay was illustrated in Fig. 5a. In the absence of let-7a, P_{let-7a} was compactly adsorbed on the surface of 2D MnO_2 nanoflakes, and thus the catalytic activity was remarkably inhibited, which led to existence of abundant MB in the solution, subsequently contributing to a high DPV peak current. Whereas, upon the addition of let-7a, it hybridized with P_{let-7a} to form P_{let-7a}@let-7a and subsequently departed from 2D MnO_2 nanoflakes due to phosphate groups-initiated shielding effect of nucleobase pairs. The removal of P_{let-7a} resulted in a significant increase in surface active sites, and thus allowed 2D MnO_2 nanoflakes to sufficiently react with MB. Given this reason, large amounts of MB was eliminated and further, a remarkably declined DPV current was acquired. Therefore, sensitive detection of let-7a can be readily achieved based on 2D MnO_2 nanoflakes-mediated homogeneous electrochemical biosensor.

To show the critical role of P_{let-7a}/MnO_2, let-7a with the concentrations of 30 nM and 100 nM were separately poured into the sensing solution, and the measured DPV curves were manifested in Fig. 5b. If no let-7a existed, the DPV peak current was recorded to be 140 nA, whereas the DPV peak current declined to 90 nA upon the addition of 30 nM let-7a, corresponding well to the sensing principle that let-7a hybridized with P_{let-7a} to form dsDNA to recover the enzyme-like activities of 2D MnO_2 nanoflakes. With the amount of let-7a further increasing to 100 nM, a lower DPV current at −0.219 V was determined, certifying that let-7a indeed give rise to decreased DPV current. Besides, the incubation time was optimized to be 15 min (Fig. S9). Similar variation can also be observed in Fig. 5c. These data firmly justified the feasibility of this proposed homogeneous biosensor for sensitively probing let-7a.

To appraise the analytical performance of P_{let-7a}/MnO_2, a plentiful of experiments were carried out and the DPV curves subjected to let-7a with different dosages were manifested in Fig. 5d. In comparison with that of blank sample (P_{let-7a}/MnO_2), DPV peak currents decreased significantly with let-7a amounts elevating in the range of 0.4–140 nM.

As a result, a standard working curve between DPV current (I) and let-7a amount ($C_{let\text{-}7a}$) was acquired with high correlation ($R^2 = 0.9853$) (Fig. 5e). The resultant equation was calculated to be $I = -1.0686C_{let\text{-}7a}+139.06$, and the detection limit (LOD) was determined to be 0.25 nM based on 3σ, which is comparable to or lower than those of previous colorimetric biosensors that were developed by nanozymes and electrochemical biosensors that were based on the bioenzymes-assisted signal amplification (Table S1). This low LOD was presumably originated from 2D MnO_2 nanoflakes' dual enzyme-like activities allowing the efficient elimination of abundant MB, 2D MnO_2 nanoflakes' superior binding to ssDNA over dsDNA and the exceptional inhibition effect of ssDNA granting a significant recovery of catalytic activity of 2D MnO_2 nanoflakes upon the addition of only a handful of let-7a. Furthermore, the batch-to-batch repeatability was explored by applying five different batches of $P_{let\text{-}7a}/MnO_2$ to probe 100 nM let-7a, and the maximum amplitude was calculated to be only 8 nA, which is very small, demonstrating the outstanding repeatability (Fig. S10).

Selectivity is a critical consideration for validating the diagnosis accuracy, and thus was inquired by using let-7b, let-7c, let-7d, miRNA-429, miRNA-21 and miRNA-16 as the interfering objects (Fig. 5f). For let-7a, the ΔI ($\Delta I = I_1 - I_0$, where I_1 is the DPV peak current of the system in the presence of one of the analytes, and I_0 is the DPV current of the blank sample) was −96 nA, which is about 2.7, 2.4, 8, 13, 16, and 11-fold higher than that of the solution in the presence of let-7b, let-7c, let-7d, miRNA-429, miRNA-21 and miRNA-16, respectively. Obviously, both let-7b and let-7c had a greater affect on output signal than let-7d, miRNA-429, miRNA-21 and miRNA-16, but also caused little interference in selective analysis of let-7a. This is not strange to us that only let-7a can hybridize with $P_{let\text{-}7a}$ to form dsDNA and subsequently depart from 2D MnO_2 nanoflakes to recover the enzyme-like activities. Thus, 2D MnO_2 nanoflakes-based homogeneous electrochemical biosensor possessed the good selectivity for discriminating let-7a against other miRNAs.

For a newly developed biosensor, another challenge is to apply it in analysis of target object in biological liquids. With this in mind, cell extract gotten from Hela cells was chosen as a representative to validate the practical application of 2D MnO_2 nanoflakes-based homogeneous electrochemical biosensor. As illustrated in Fig. 5g, upon the addition of cell extract into the sensing system (the final concentration of Hela cell is 1.0×10^4 cell/μL), the output signal negligibly varied compared with the blank sample and indicated that the expression level of let-7a in cell extract is too low to be detected by our biosensor, corresponding well to previously reported work (Shi et al., 2019). With 5 nM let-7a being added, the sensing system emitted declined fluorescence; with the amount of let-7a further raising, the fluorescence signal continued to decrease. According to the linear equation, the measured values by our biosensor were 5.27 nM, 14.45 nM and 30.63 nM, respectively, the mean recoveries were calculated to be 105.4%, 96.3%, and 102.1%, and the relative standard deviations (RSDs) were calculated to be 5.48%, 3.82% and 2.47%, respectively (Table S2). More importantly, the measured values kept high line with that of reverse transcription-polymerase chain reaction (RT-PCR). These data justified the great potential application of our biosensor for practical miRNA analysis in medical field.

3. Conclusions

In summary, 2D MnO_2 nanoflakes with ultrathin thickness were successfully prepared through a soft template-directed wet chemical approach. After the catalytic activity and morphology tests, 2D MnO_2 nanoflakes were found to have the oxidase- and peroxidase-like activities, and the activity and morphology can be easily tuned by varying the dosage of MES. Profiting from the dual enzyme-like activities, 2D MnO_2 nanoflakes demonstrated a high activity to catalyze oxidation of O_2 into ROS and significantly decrease the DPV peak current through eliminating MB. Moreover, 2D MnO_2 nanoflakes displayed a unique response to ssDNA. Owing to ssDNA-sensitivity and dual enzyme-like activities, a 2D MnO_2 nanoflakes-based homogeneous electrochemical biosensor for miRNA was developed with a good linear range from 0.4 to 100 nM for let-7a. This typical 2D nanozyme sets up a new avenue for developing higher-performance homogeneous electrochemical biosensors, supplying significant prospects for further construction of MB-based homogeneous electrochemical system.

CRediT authorship contribution statement

Jiahui Wu: Conceptualization, Data curation, Investigation, Methodology, Writing - original draft. **Wenxin Lv:** Conceptualization, Investigation, Methodology. **Qiaoting Yang:** Conceptualization, Data curation, Investigation, Methodology. **Haiyin Li:** Conceptualization, Project administration, Software, Supervision, Resources, Writing - review & editing. **Feng Li:** Funding acquisition, Project administration, Resources.

Declaration of competing interest

The authors declare that they have no known competing financial interests or personal relationships that could have appeared to influence the work reported in this paper.

Acknowledgements

This work was financially supported by National Natural Science Foundation of China (21605093 and 21775082), the Shandong Province Higher Educational Program for Young Innovation Talents, the Major Program of Shandong Province Natural Science Foundation (ZR2018ZC0127), and the Special Foundation for Distinguished Taishan Scholar of Shandong Province (ts201511052).

Appendix A. Supplementary data

Supplementary data to this article can be found online at https://doi.org/10.1016/j.bios.2020.112707.

References

Bai, Y.Y., Wu, Z., Xu, C.M., Zhang, L., Feng, J., Pang, D.W., Zhang, Z.L., 2020. Anal. Chem. 92 (1), 853–858.
Chang, J.F., Lv, W.X., Li, Q., Li, H.Y., Li, F., 2020. Anal. Chem. 92, 8959–8964.
Chen, Q., Chen, J., Yang, Z., Xu, J., Xu, L., Liang, C., Han, X., Liu, V.Z., 2019. Adv. Mater. 31 (10), 1802228.
Fu, L.H., Qi, C., Hu, Y.R., Lin, J., Huang, P., 2019. Adv. Mater. 31 (21), 1808325.
Hou, T., Li, W., Liu, X., Li, F., 2015. Anal. Chem. 87 (22), 11368–11374.
Huang, Y.Y., Ren, J.S., Qu, X.G., 2019. Chem. Rev. 119 (6), 4357–4412.
Han, L., Zhang, H.J., Chen, D.Y., Li, F., 2018. Adv. Funct. Mater. 28 (17), 1800018.
Jong, M.D., Sleegers, N., Kim, J., Durme, F.V., Samyn, N., Wang, J., Wael, K.D., 2016. Chem. Sci. 7 (3), 2364–2370.
Kang, X., Zhu, M.Z., 2019. Small 15 (43), 1970230.
Kim, M.S., Lee, J., Kim, H.S., Cho, A., Shim, K.H., Le, T.N., An, S.S.A., Han, J.W., Kim, M. I., Lee, J., 2020. Adv. Funct. Mater. 30 (1), 1905410.
Lin, T., Rapino, S., Girault, H.H., 2018. Chem. Sci. 9 (20), 4546–4554.
Li, H.Y., Lin, H.Y., Lv, W.X., Gai, P.P., Li, F., 2020. Biosens. Bioelectron. 165, 112336.
Li, S., Zhao, X.T., Yu, X.X., Wan, Y.Q., Yin, M.Y., Zhang, W.W., Cao, B.Q., Wang, H., 2019. Anal. Chem. 91 (22), 14737–14742.
Liu, Z.W., Wang, F.M., Ren, J.S., Qu, X.G., 2019. Biomaterials 208, 21–31.
Liu, M., Zhao, H.M., Chen, S., Yu, H.T., Quan, X., 2012. ACS Nano 6 (4), 3142–3151.
Liu, Y., Ding, D., Zhen, Y.L., Guo, R., 2017. Biosens. Bioelectron. 92, 140–146.
Martinfernandez, B., Manzanarespalenzuela, C.L., Lopez, M.S., Delossantosalvarez, N., Lopezruiz, B., 2017. Crit. Rev. Food Sci. Nutr. 57 (13), 2758–2774.
Palomo, J.M., 2019. Chem. Commun. 55 (65), 9583–9589.
Qiu, H., Pu, F., Ran, X., Liu, C.Q., Ren, J.S., Qu, X.G., 2018. Anal. Chem. 90 (20), 11775–11779.
Shi, C.X., Li, S.X., Chen, Z.P., Liu, Q., Yu, R.Q., 2019. Anal. Chem. 91 (3), 2120–2127.
Silva, N.F., Magalhaes, J.M., Freire, C., Deleruematos, C., 2018. Biosens. Bioelectron. 99, 667–682.
Singh, N., Savanur, M.A., Srivastava, S., Dsilva, P., Mugesh, G., 2017. Angew. Chem. Int. Ed. 56 (45), 14267–14271.
Taylor, A.W., Puttick, S., Licence, P., 2012. J. Am. Chem. Soc. 134 (38), 15636–15639.
Wang, Q.Q., Chen, M.X., Lin, P.H., Cui, Z.Q., Chu, C.L., Shen, B.L., 2018. J. Am. Chem. Soc. 6 (23), 10686–10699.

Wiedmer, D., Sagstuen, E., Welch, K., Haugen, H.J., Tiainen, H., 2016. Appl. Catal. B Environ. 198, 9–15.
Wu, J.J.X., Wang, X.Y., Wang, Q., Lou, Z.P., Li, S.R., Zhu, Y.Y., Qin, L., Wei, H., 2019. Chem. Soc. Rev. 48, 1004–1076.
Wang, X.C., Lv, F., Li, T., Han, Y.M., Yi, Z.F., Liu, M.Y., Chang, J., Wu, C.T., 2017. ACS Nano 11 (11), 11337–11349.
Weerathunge, P., Ramanathan, R., Torok, V.A., Hodgson, K.R., Xu, Y., Goodacre, R., Behera, B.K., Bansal, V., 2019. Anal. Chem. 91 (5), 3270–3276.
Xing, S.T., Zhou, Z.C., Ma, Z.C., Wu, Y.S., 2011. Appl. Catal. B Environ. 107 (3), 386–392.
Xi, J.Q., Wei, G., An, L.F., Xu, Z.B., Xu, Z.L., Fan, L., Gao, L.Z., 2019. Nano Lett. 19 (11), 7645–7654.
Yan, Y., Zeitler, E.L., Gu, J., Hu, Y., Bocarsly, A.B., 2013. J. Am. Chem. Soc. 135 (38), 14020–14023.
Zhang, F.T., Nie, J., Zhang, D.W., Chen, J.T., Zhou, Y.L., Zhang, X.X., 2014. Anal. Chem. 86 (19), 9489–9495.
Zhao, F., Liu, L.F., Yang, F.L., Ren, N.Q., 2013. Chem. Eng. J. 230, 491–498.
Zhang, J.Y., Wu, S.H., Lu, X.M., Wu, P., Liu, J.W., 2019. Nano Lett. 19 (5), 3214–3220.
Zhou, Y., Wang, L., Ye, Z., Zhao, M., Huang, J., 2014. Electrochim. Acta 115, 277–282.